doi:10.1016/j.jmb.2009.01.035 J. Mol. Biol. (2009) 387, 207–218

JMB

Available online at www.sciencedirect.com

ScienceDirect

ELSEVIER

The β_E-Domain of Wheat E_c-1 Metallothionein: A Metal-Binding Domain with a Distinctive Structure

Estevão A. Peroza[1], Roland Schmucki[2,3], Peter Güntert[2,3], Eva Freisinger[1]* and Oliver Zerbe[4]*

[1]*Institute of Inorganic Chemistry, University of Zürich, Winterthurerstr. 190, CH-8057 Zürich, Switzerland*

[2]*Institute of Biophysical Chemistry, Goethe-University Frankfurt am Main, Max-von-Laue-Str. 9, 60438 Frankfurt am Main, Germany*

[3]*Frankfurt Institute for Advanced Studies, Ruth-Moufang-Str. 1, 60438 Frankfurt am Main, Germany*

[4]*Institute of Organic Chemistry, University of Zürich, Winterthurerstr. 190, CH-8057 Zürich, Switzerland*

Received 16 November 2008; received in revised form 19 January 2009; accepted 20 January 2009
Available online 27 January 2009

Edited by M. F. Summers

Metallothioneins (MTs) are ubiquitous cysteine-rich proteins with a high affinity for divalent metal ions such as Zn^{II}, Cu^{I}, and Cd^{II} that are involved in metal ion homeostasis and detoxification, as well as protection against reactive oxygen species. Here we show the NMR solution structure of the β_E-domain of the early cysteine-labeled protein (E_c-1) from wheat (β_E-E_c-1), which represents the first three-dimensional structure of a plant MT. The β_E-domain comprises the 51 C-terminal residues of E_c-1 and exhibits a distinctive unprecedented structure with two separate metal-binding centers, a mononuclear Zn^{II} binding site constituted by two cysteine and two highly conserved histidine residues as found in certain zinc-finger motifs, and a cluster formed by three Zn^{II} ions coordinated by nine Cys residues that resembles the cluster in the β-domain of vertebrate MTs. Cys–metal ion connectivities were determined by exhaustive structure calculations for all 7560 possible configurations of the three-metal cluster. Backbone dynamics investigated by ^{15}N relaxation experiments support the results of the structure determination in that β_E-E_c-1 is a rigidly folded polypeptide. To further investigate the influence of metal ion binding on the stability of the structure, we replaced Zn^{II} with Cd^{II} ions and examined the effects of metal ion release on incubation with a metal ion chelator.

Keywords: plant metallothionein; zinc; metal cluster; NMR; histidine ligands

Introduction

Metallothioneins (MTs) are cysteine-rich proteins that display a high affinity for metal ions such as Zn^{II}, Cu^{I}, and Cd^{II}. These proteinogenic metal chelators are widely spread in nature, occurring in the most diverse living organisms (e.g., vertebrates, bacteria, fungi, and plants).[1] Although their biological role is still debated, several functions have already been attributed to MTs, among them participation in metal ion homeostasis and detoxification, as well as protection against reactive oxygen species.[2,3]

MTs generally coordinate metal ions via the thiolate moiety of their cysteine residues, resulting in the formation of metal–thiolate clusters. Only two different cluster arrangements for divalent metal ions have been structurally characterized so far: the M_3Cys_9 cluster of the β-domain of vertebrate, crustacean, and echinodermata MTs, and the M_4Cys_{11} cluster of the α-domain of vertebrate and echinodermata MTs.[4–12] A variant of this four-metal ion cluster—in which two histidine residues participate

*Corresponding authors. E-mail addresses: freisinger@aci.uzh.ch; oliver.zerbe@oci.uzh.ch.

Abbreviations used: MT, metallothionein; E_c-1, early cysteine-labeled protein; ABA, abscisic acid; β_E-E_c-1, β_E-domain of wheat E_c-1; 3D, three-dimensional; HSQC, heteronuclear single-quantum coherence; TOCSY, total correlation spectroscopy; NOE, nuclear Overhauser effect; NOESY, NOE spectroscopy; 2D, two-dimensional; PAR, 4-(2-pyridylazo)-resorcinol.

in metal ion coordination, resulting in a $M_4Cys_9His_2$-type arrangement—has been described to occur in cyanobacteria *Synechococcus* sp. PCC 7942.[13]

MTs are classified into 15 families according to sequence similarities and phylogenetic relationships.[14] Plant MTs compose family number 15 and are further divided into four main subfamilies p1, p2, p3, and pec, mainly based on the distribution of Cys residues in the Cys-rich regions of the amino acid chain. Members of the pec subfamily contain 17 Cys residues concentrated in three regions of the primary sequence separated by two Cys-free stretches that are 14 and 15 amino acids in length, respectively (Fig. 1). The presence of three Cys-rich regions distinguishes the pec proteins from the members of the other three plant MT subfamilies that contain only two cysteine-rich stretches. A second distinctive feature is the absence of any aromatic amino acid other than His residues from the pec proteins, while the MTs from the p1, p2, and p3 subfamilies can also contain the aromatic amino acids Phe and Tyr in their long Cys-free linker regions. Expression of the E_c proteins is restricted to developing seeds, as well as to embryogenic microspores and pollen embryoids.[15]

The early cysteine-labeled protein (E_c-1) from bread wheat (*Triticum aestivum*) is a typical member of the pec subfamily and was the first MT to be identified in higher plants.[16–18] The protein owes its name to the fact that, with a content of 20–25%, it is the principal site of Cys incorporation during the first hour of germination of the wheat embryo.[16] However, it was later found that accumulation of E_c-1 mRNA is even greater in immature embryos approximately 15 days postanthesis and shows declining levels as embryogenesis progresses.[17] E_c-1 mRNA concentrations decline rapidly after 1 h of imbibition, and no more coding mRNA can be detected after 5 h. In contrast to other MTs, it seems unlikely that wheat E_c-1 plays a role in the detoxification of metal ions because the 5′ flanking region of the gene was found to be devoid of any metal-responsive element known from mammalian counterparts. Accordingly, incubation with Zn^{II} or Cd^{II} ions does not lead to induction of E_c-1. In contrast, a promoter sequence with homology to abscisic acid (ABA)-responsive elements was identified, and ABA is indeed a strong inducer of E_c-1 gene transcription. ABA is a plant hormone that is responsible for, among others, seed dormancy by inhibiting cell growth and, thus, seed germination. Wheat E_c-1 can be isolated from wheat germs as a zinc-binding protein[18] and was therefore suggested to be involved in the regulation of zinc levels during embryogenesis.[17] Considering that zinc concentrations in the developing seed are highest both in the embryo and in the aleurone layer,[19] E_c-1, in addition to phytate, is expected to be the major Zn^{II} binding partner also in the latter tissue. Diminishing E_c-1 mRNA concentrations correlate well with remobilization of zinc into the newly emerging root tips and coleoptile, and suggest a zinc storage function for E_c-1. We previously demonstrated that wheat E_c-1 has a high affinity for up to six divalent metal ions, and we raised strong evidence that the metal ions are arranged in two separated metal-binding domains.[20] E_c-1 is able to coordinate two divalent metal ions via the six Cys residues of its N-terminal γ-domain, presumably forming a Zn_2Cys_6 cluster, which has never been reported before in any other MT. The C-terminal domain of wheat E_c-1 comprises the central and C-terminal Cys-rich regions, with a total of 11 cysteine and 2 histidine residues as potential ligands for the four divalent metal ions found to be coordinated to this part of the protein (Fig. 1). We designate the C-terminal domain of wheat E_c-1 as the β_E-domain or expanded β-domain due to the results of the structure investigation presented in the following. Despite the broad knowledge on vertebrate MT isoforms accumulated over the past 50 years, plant MTs form still a comprehensive research field in need of further exploration. Here we present the solution structure of the β_E-domain of wheat E_c-1 (β_E-E_c-1), representing the first three-dimensional (3D) structure of a plant MT. The β_E-domain exhibits two separate metal centers. One cluster contains three metal ions coordinated to nine Cys residues, resembling the cluster of the β-domain of vertebrate isoforms. An additional mononuclear binding site constitutes of two cysteine and two histidine residues, as known, for example, from zinc-finger proteins, a motif previously unknown to occur in MTs. In addition, we performed ^{15}N relaxation experiments to investigate backbone dynamics. These data corroborate results from structure determination in that the Zn^{II} form of β_E-E_c-1 is a rigidly folded polypeptide. To further investigate the role of metal ion binding in stabilizing the structure, we replaced Zn^{II} with Cd^{II} ions and examined the effects of metal ion release on incubation with a metal ion chelator.

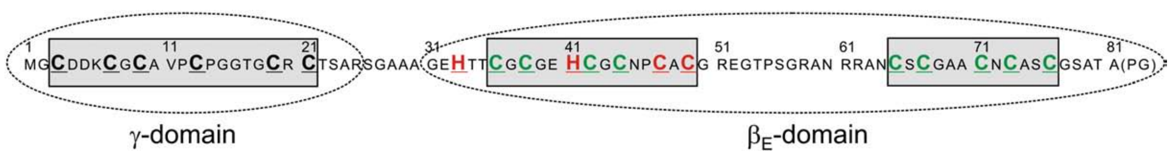

Fig. 1. Amino acid sequence of full-length wheat E_c-1. Zn^{II}-coordinating Cys and His residues are indicated with bold and larger letters. Residues belonging to the γ- and β_E-domains are marked with two dotted ellipsoids, and the three Cys-rich regions are marked with gray-shaded boxes. Residues highlighted in red and green indicate their participation in the mononuclear Zn^{II} binding site and the three-Zn^{II} ion cluster, respectively. The two C-terminal amino acids PG are artificially introduced by the cloning strategy used.

Results

Resonance assignments

The solution structure of $Zn_4\beta_E$-E_c-1 was determined at pH 6.8 and 300 K using a recombinantly produced uniformly ^{15}N-labeled sample. A [^{15}N,^{1}H]-heteronuclear single-quantum coherence (HSQC) spectrum of β_E-E_c-1 is shown in Fig. 2. The spectrum displays good signal dispersion and sharp lines, indicating that conformational exchange processes are largely absent in the Zn^{II} isoform. Resonance assignment was accomplished following the traditional sequential sequence-specific resonance assignment strategy. Spin systems were recognized in the 3D ^{15}N-resolved [^{1}H,^{1}H]-total correlation spectroscopy (TOCSY) spectrum and mainly linked via sequential αN nuclear Overhauser effects (NOEs) from the 3D ^{15}N-resolved [^{1}H,^{1}H]-NOE spectroscopy (NOESY) spectrum (see Fig. S1). Due to good signal dispersion, this approach was successful, and all backbone and nonlabile side-chain ^{1}H resonances and the corresponding ^{15}N chemical shifts could be assigned without exception. Only a few labile protons remained unassigned (Table S2).

Metal ion coordination determination

The topology of the metal ion binding sites has traditionally been established by measuring scalar couplings between (mainly H^{β}) protons of Cys and the metal ions.[21–24] Since Zn^{II} is not a nucleus with favorable NMR properties, it was replaced with $^{113}Cd^{II}$ in previous studies. Either two-dimensional (2D) [^{113}Cd,^{113}Cd]-correlation spectroscopy[6] and ^{113}Cd homodecoupling techniques,[17,18] or ^{113}Cd,^{1}H correlation experiments[22] were performed after replacing Zn^{II} with $^{113}Cd^{II}$. In the case of β_E-E_c-1, unfortunately, the ^{113}Cd NMR spectra displayed broad lines, presumably due to kinetic instability of the metal cluster, and the ^{113}Cd,^{1}H correlation spectra lacked interpretable signals. All ^{113}Cd spectra and [^{113}Cd,^{1}H]-HSQC experiments were performed at a ^{1}H frequency of 500 MHz, ruling out the chemical shift anisotropy mechanism as a major source of line broadening. In addition, [^{15}N,^{1}H]-HSQC spectra of ^{113}Cd-subsituted β_E-E_c-1 were identical at protein concentrations of 1 and 3 mM. Therefore, we applied a different computational method to determine metal–thiolate connectivities.

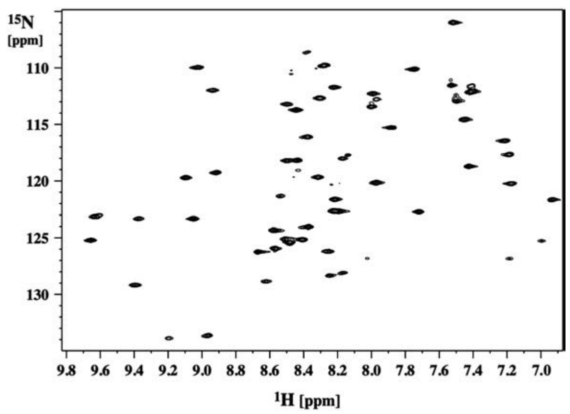

Fig. 2. [^{15}N,^{1}H]-HSQC spectrum of $Zn_4\beta_E$-E_c-1 recorded at 600 MHz proton frequency and 300 K.

We first performed structure calculations using automated NOE assignment[25] without considering the presence of the metal ions. The resulting preliminary structure was sufficiently well-defined to show that a single metal ion is coordinated by His33, His41, Cys47, and Cys49 (see Fig. S3). Although no interresidual NOE involving β-protons of different Cys residues was observed, 42 NOEs between amide or α protons of two different Cys residues were detected. The chemical shifts of the atoms in the aromatic rings of the His residues identified $N^{\delta1}$ of His33 and $N^{\varepsilon2}$ of His41 as the atoms coordinating a single Zn^{II} ion (see Fig. S4). The remaining nine Cys residues can form a cluster with three equivalent metal ions, three bridging Cys (binding two metal ions each), and 3×2 terminal Cys (binding one metal ion each) as found in the β-domains of vertebrate MTs in $(9\times8\times7)/6\times(6\times5)/2\times(4\times3)/2\times(2\times1)/2=7560$ different ways, excluding symmetrically related arrangements. Using the program CYANA, we performed for each of the 7560 possible cluster arrangements a complete structure calculation with automated NOE assignment and ranked the resulting structure bundles by their final target function value. During the structure calculations, tetrahedral coordination geometry around the metal sites was assumed. In addition, we ran 3×7560 structure calculations with fixed NOE upper distance limits that had resulted from three of the aforementioned automated NOE assignment and structure calculations without metal ions started from different randomized initial structures. All structure calculations with automated NOE assignment used the same input peak lists containing 607 and 1039 cross-peaks from 3D ^{15}N-resolved NOESY and 2D homonuclear NOESY, respectively. Structure calculations were completed in about 5 days using up to 100 processors of a Linux cluster system in parallel.

Low target function values that indicate compatibility with experimental NMR data and good stereochemistry were observed for several of the 7560 possible cluster configurations. The lowest target function value was realized in three out of the four aforementioned calculations (in one of three structure calculations with fixed NOE assignments, it ranked second out of 7560) by a three-metal cluster configuration, with Cys36, Cys38, Cys67, and Cys71 coordinating a first metal ion, with Cys36, Cys44, Cys73, and Cys76 coordinating a second metal ion, and with Cys42, Cys65, Cys67, and Cys76 coordinating a third metal ion. We chose this configuration of the three-metal cluster as representative of the solution structure of β_E-E_c-1. However, other Cys–Zn coordinations are almost equally compatible with the NMR data. In Supplementary Material, the 10 configurations of the three-metal cluster with the lowest maximal rank are listed as sorted by the final target function value over all 7560 possible cases in each of the four calculations (Table S10). The fact that structure calculations, on the basis of the available conformational restraints from NMR data, cannot unambiguously define the configuration of the Zn_3Cys_9 cluster may reflect the presence of dynamic exchange processes between multiple configurations with different Cys–Zn coordinations, in agreement with the broad lines observed in the ^{113}Cd,^{1}H correlation spectra. Notably, different low-energy cluster configurations result in only limited variation of the backbone structure of the protein, as reflected by average backbone RMSD values of 1.4 Å between the representative structure and the structures with other cluster configurations listed in Table S10. Of the nine Cys residues that form the three-metal cluster, most occur both as bridging and terminal cysteines in these 10 cluster configurations of Table S10. Strong preferences could be observed for Cys38, Cys44, and Cys65, which occur as terminal cysteines in 90% or more of the cases.

Solution structure of $Zn_4\beta_E$-E_c-1

The solution structure of $Zn_4\beta_E$-E_c-1 is depicted in Fig. 3 (see also Fig. S5). The most striking feature is the presence of a Zn_3Cys_9 cluster separated from a mononuclear binding site, with the latter never having been reported for MTs before. Particularly interesting is the observation that the amino acids forming the isolated binding site are, to a certain extent, interleaved with the positions of the Cys ligands constituting the Zn_3Cys_9 cluster. The single metal ion binding site is constituted by His33, His41, Cys47, and Cys49 of the N-terminal Cys-rich region of $Zn_4\beta_E$-E_c-1, and hence part of the central Cys-rich region in the full-length E_c-1. Such $ZnCys_2His_2$ sites were so far only known from, for example, zinc-finger proteins, where they play a structural role for the recognition of DNA.[26] The remaining nine cysteine residues that originate from the N-terminal (Cys36, Cys38, Cys42, and Cys44) and C-terminal (Cys65, Cys67, Cys71, Cys73, and Cys76) Cys-rich regions of $Zn_4\beta_E$-E_c-1 form a three-metal cluster with a stoichiometry also observed in the β-domain of the vertebrate MTs. The fact that residues relatively far apart in the primary sequence come together to form two distinct metal ion binding sites results in a compact arrangement of the two sites. This structure is surrounded by a long loop formed by the residues between Gly50 and Asn64. Strikingly, the adjacent residues His41 and Cys42 take part in the formation of different metal ion binding sites. A short α-helical element is observed in the segment from Ala74 to Gly77, which includes the Zn-coordinating residue Cys76.

MTs are, in general, largely devoid of secondary structure, and the rigidity of their backbone is mainly due to metal ion coordination by Cys or His residues. To further support the existence of the isolated metal ion binding site, we measured backbone dynamics through ^{15}N relaxation experiments. The values of the longitudinal relaxation times (T_1), transverse relaxation times (T_2), and ^{15}N{^{1}H}-NOEs are depicted in Fig. 4. The data reveal that the polypeptide is rigidly structured, with the exception of the first two residues and the last five residues. Otherwise, T_1, T_2, and the heteronuclear ^{15}N{^{1}H} NOE values are comparably uniform along the sequence. In particular, the position of His33, postulated here to be one of the ligands of the isolated cluster, is already rigidly folded. Considering the absence of secondary structure in most MTs, this clearly argues for His33 to take part in metal ion coordination. It is not unexpected that the N-terminal residues are already rigidly structured because the sequence boundary of the β_E-domain was derived based on proteolytic digestion experiments with proteinase K.[20] Proteinase K has been shown to cleave the peptide backbone of MTs in regions not protected by metal–thiolate clusters. Hence, the more flexible N-terminal residues of the β_E-domain not involved in cluster formation were removed by proteinase K digestion.

Comparison of $Zn_4\beta_E$-E_c-1 and $Cd_4\beta_E$-E_c-1

MTs can bind divalent metal ions, and complexation to both Zn^{II} and Cd^{II} occurs with high affinity. While the Cd–S bond is thermodynamically more stable than the corresponding Zn–S bond, Cd–S

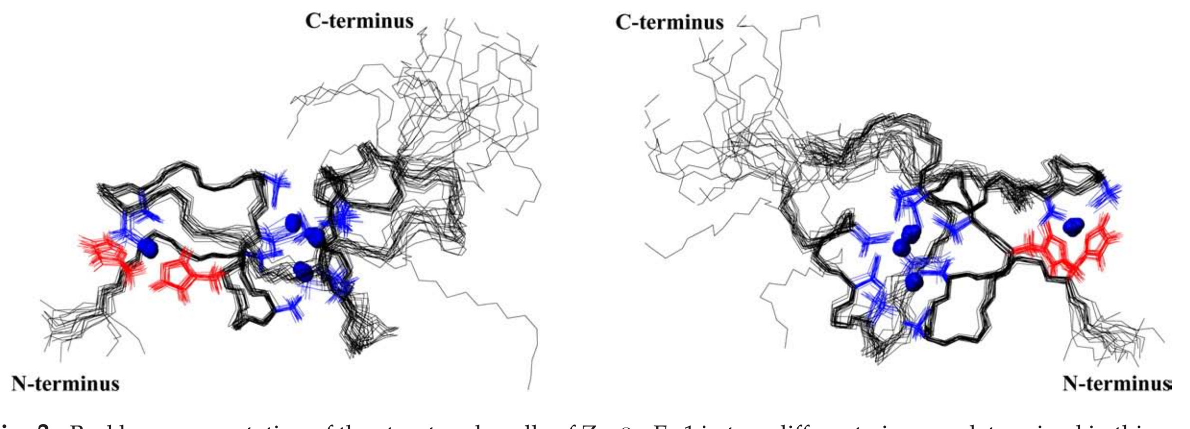

Fig. 3. Backbone presentation of the structure bundle of $Zn_4\beta_E$-E_c-1 in two different views as determined in this work. His and Cys side chains are additionally shown in red and blue, respectively, and Zn^{II} ions are shown as blue spheres.

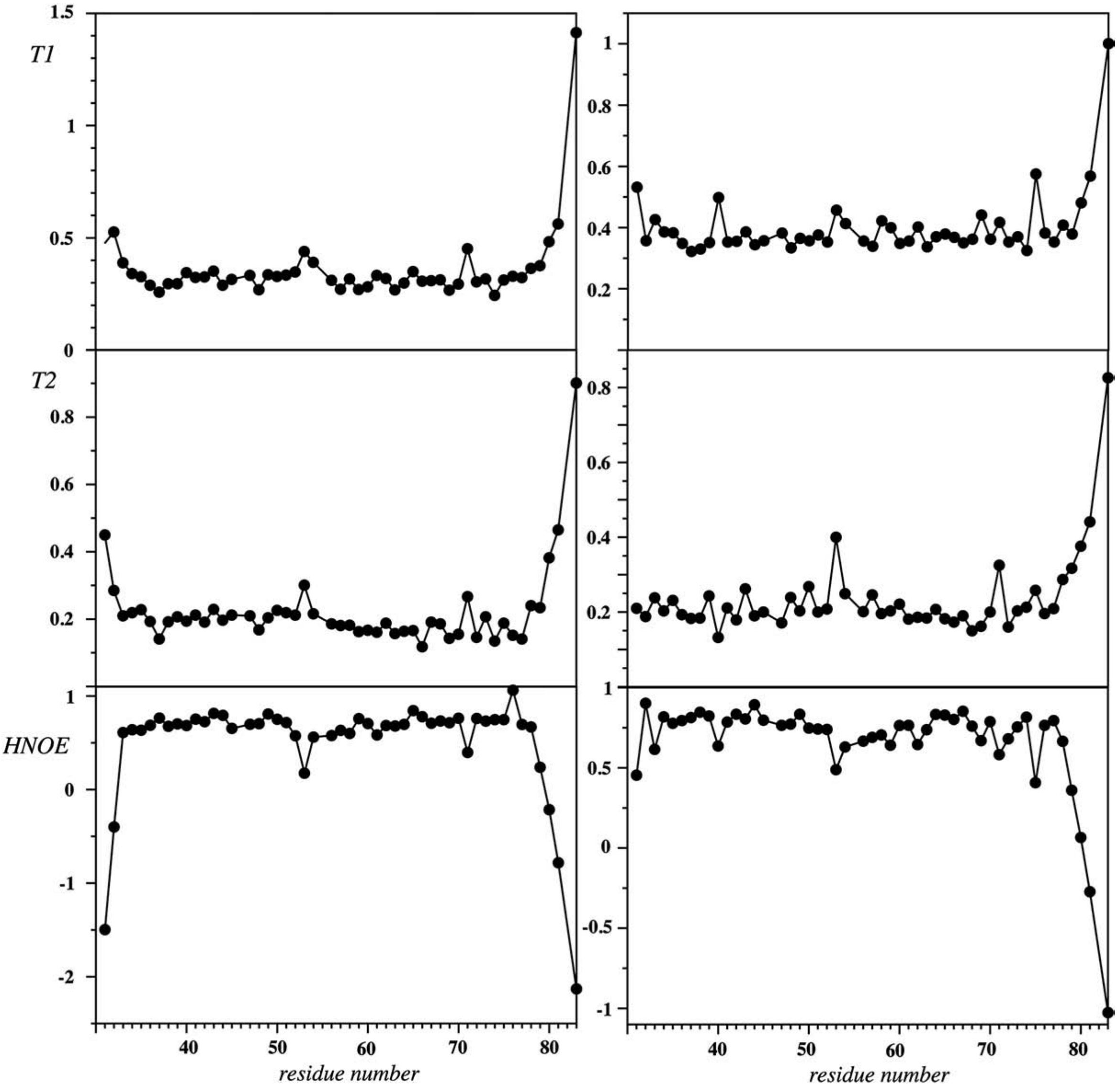

Fig. 4. Relaxation parameter of β in Zn^{II}- (left) and Cd^{II}-loaded forms (right). Depicted are values of T_1 (top), T_2 (middle), and $^{15}N\{^1H\}$ NOE (bottom). Data were measured at 700 MHz proton frequency and 300 K on 1 mM $Zn_4\beta_E$-E_c-1 and 3 mM $^{113}Cd_4\beta_E$-E_c-1 samples.

clusters are often kinetically labile.[27,28] Due to the difference in ion radii, Cd_n–S_m clusters occupy a significantly larger volume than the corresponding Zn species.[29] Zn^{II} and Cd^{II} in mixed-metal Zn,Cd MTs have been shown to partition nonstatistically into the two different domains, with Zn^{II} being preferentially bound in the three-metal cluster and with Cd^{II} being preferentially bound in the four-metal cluster.[28,30] Despite these differences, Zn^{II}–Cd^{II} metal ion exchange has often been used to introduce an NMR active probe into the system.[22] We have used ^{15}N–^1H correlation spectroscopy to investigate whether the Zn^{II}- and Cd^{II}-loaded isoforms display similar structural and dynamical features.

The [^{15}N,^1H]HSQC spectrum of $^{113}Cd_4$-β_E-E_c-1, although similar to that of the Zn^{II} isoform, contains additional minor peaks (Fig. S6). The linewidths for the Cd^{II}-loaded species are larger, and additional very broad signals in the random coil range occur. We attribute these spectroscopic features to the presence of multiple conformers, mainly due to kinetic instability of the Cd^{II} isoform. This view is supported by the fact that Cd^{II}–thiolate clusters in MTs are kinetically more labile than the corresponding Zn^{II} species.[31,32] During the structure calculations, we noticed that small conformational alterations reflected by tiny changes in energy are required to modify metal complexation modes in the three-metal cluster (*vide supra*). Taking the kinetic instability of the Cd–S bond into account, this may explain the well-known dynamic nature of Cd_3S_9 clusters[33] and may point to a general problem of determining metal–Cys coordination modes from cadmium–proton correlation spectroscopy in such unfavorable cases. We also noticed that the additional broad peaks observed in the Cd^{II} sample also appeared when the metal ion chelator 4-(2-pyridylazo)-

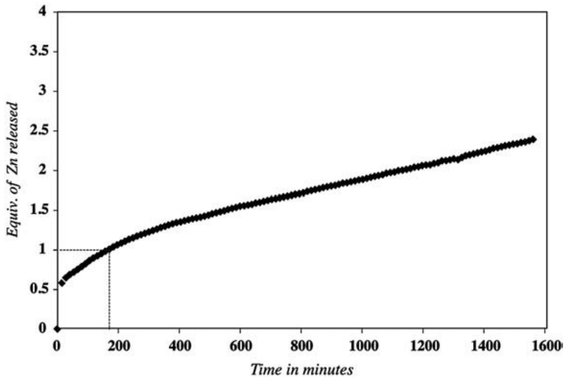

Fig. 5. Zn^{II} release from the $Zn_4\beta_E$-E_c-1 upon incubation with a 120-fold excess of PAR at 12 °C, followed by UV spectroscopy. Dashed lines indicate the time when the first equivalent of Zn^{II} was removed from the domain.

resorcinol (PAR) was added to the Zn^{II} isoform (*vide infra*). The ^{113}Cd NMR spectra of full-length wheat MT E_c-1 revealed that resonances of the β-domain occur at almost identical positions and with comparable linewidths,[34] ruling out that destabilization occurs in the truncated β_E-domain. A comparison of the amide proton and amide nitrogen chemical shifts between the Zn^{II}-loaded species and the Cd^{II}-loaded species revealed significant chemical shift changes in the vicinity of the metal-ion-coordinating residues of the three-metal cluster, especially in the C-terminal cysteine-rich region (Fig. S7). The chemical shift differences for other residues are small, suggesting that the overall architecture is very similar.

The ^{15}N relaxation data recorded on the $^{113}Cd_4\beta_E$-E_c-1 sample are similar to those of the $Zn_4\beta_E$-E_c-1 sample (Fig. 4), indicating that despite the kinetic lability of metal ion coordination in the Cd^{II}-substituted isoform, both polypeptides are similarly rigid on the timescale of the ^{15}N relaxation experiments. Exchange processes can possibly contribute to T_2 relaxation, but the fact that no significant effect is observed in this case indicates that the exchange processes are in the slow NMR time regime for ^{15}N while in intermediate exchange for ^{113}Cd nuclei. The fact that two sets of signals are observed in the [^{15}N,^{1}H]HSQC spectra supports this view.

Demetalation experiments

Whereas the apo forms of MTs feature a high degree of random coil structure,[35,36] the structures of holo-MTs are predominantly stabilized by interactions between the cysteine thiolate groups and the coordinated metal ions. Cluster formation in MTs was postulated to be highly cooperative,[37–39] although this has recently been questioned for human MT-1a based on mass spectrometric analysis.[40] To investigate the influence of partial demetalation on the 3D structure, $Zn_4\beta_E$-E_c-1 was incubated with PAR, a chelator forming $Zn(PAR)_2$ complexes. Figure 5 illustrates the time-dependent metal ion transfer reaction followed by UV spectroscopy. As evident from the absorption at 500 nm, the first equivalent of Zn^{II} is removed after approximately 200 min at room temperature. A maximum of almost 2.5 Eq of Zn^{II} is released upon further incubation for over 26 h. To investigate the amount of structural changes taking place upon metal ion release, the same reaction was monitored by ^{15}N–^{1}H correlation spectroscopy under the same conditions of concentration, pH, and temperature. The volumes of peaks from the natively folded protein decreased exponentially over time with an approximately uniform rate, concomitant with the appearance of new additional peaks in the random coil range between 8 and 8.5 ppm (Supplementary Material, Fig. S8). Most of the cross-peak volume decrease takes place already during the first 200 min of incubation and can thus be correlated with the release of the first Zn^{II} ion from the β_E-domain detected by UV spectroscopy. This suggests that the release of a just 1 Eq of Zn^{II} from the domain is sufficient to trigger destabilization of the entire structure and supports the view that metal-induced folding of MTs is highly cooperative. Our data do not support a model in which the first metal ion is removed from a distinct metal binding site.

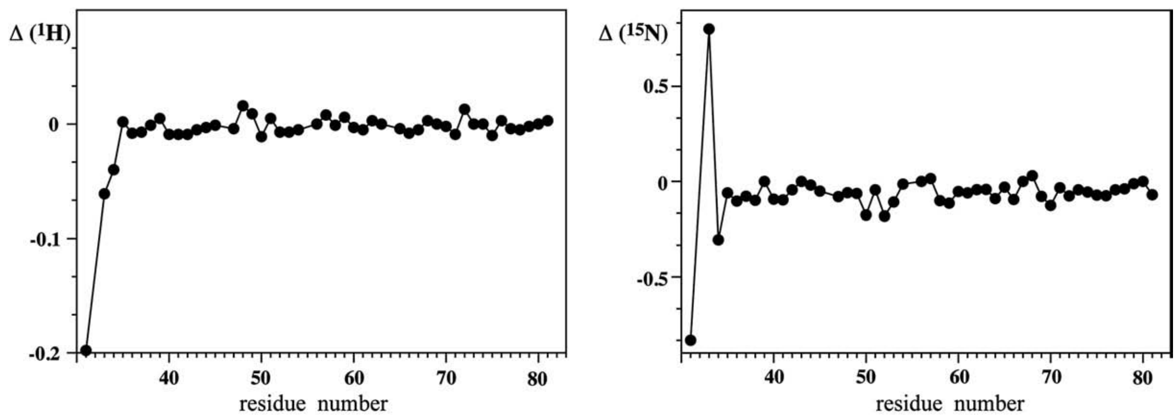

Fig. 6. Differences between the chemical shifts of the backbone amide protons (left) and nitrogen atoms (right) in the 53-residue C-terminal segment of Zn_6E_c-1 and in $Zn_4\beta_E$-E_c-1.

Comparison to full-length Zn_6E_c-1

To investigate to which extent the conformation of the C-terminal β_E-domain of E_c-1 is influenced by truncation of the polypeptide sequence, we have compared the full-length protein and the β_E-domain by heteronuclear NMR. The corresponding [^{15}N,^{1}H] HSQC spectra reveal almost identical resonance positions for the 53-residue C-terminal segment (Fig. 6; Fig. S9). Chemical shift differences are largely limited to the N-terminal tetrapeptide of β_E-E_c-1, for which changes are expected because of its proximity to the truncation site. The close match of the backbone amide proton and nitrogen frequencies between $Zn_4\beta_E$-E_c-1 and the corresponding segment in the full-length E_c-1 protein indicates that the architecture of the β_E-domain is very similar, and that the mode of metal ion coordination most likely has not changed in the truncated construct.

The $^{15}N\{^{1}H\}$ NOE unveils that the N-terminal portion of the full-length protein containing the γ-domain and the connecting linker is slightly less rigidly folded than the C-terminal portion (Fig. 7, in gray). The residues Thr21-Ala29 around the two proteolytic cleavage sites between residues Arg25/Ser26 and Ala30/Gly31 described in Lane *et al.* are highly flexible, with values of the hetereonuclear NOE approaching zero.[18] These data clearly show that the full-length protein is divided into two well-structured domains separated by a flexible linker. Only in case of the crystal structure of rat MT-2 was the relative orientation of the two domains defined,[41] which was suggested to be due to binding of phosphate in the solid state.[42] In this respect, the wheat E_c-1 protein resembles the general architecture of vertebrate MTs. However, the 14-residue linker region between the γ-domain and the β_E-domain of E_c-1 is much longer than the three-amino-acid stretch found in the vertebrate forms. Considering that α- and β-domains are separated by flexible linkers in other MTs investigated so far, this indicates that our truncated construct constitutes the entire C-terminal β_E-domain. This view is additionally supported by the fact that proteolysis yielded exactly this polypeptide. The ^{15}N relaxation experiments further show that the β_E-domain is structurally slightly more rigid than the N-terminal γ-domain (Fig. 7).

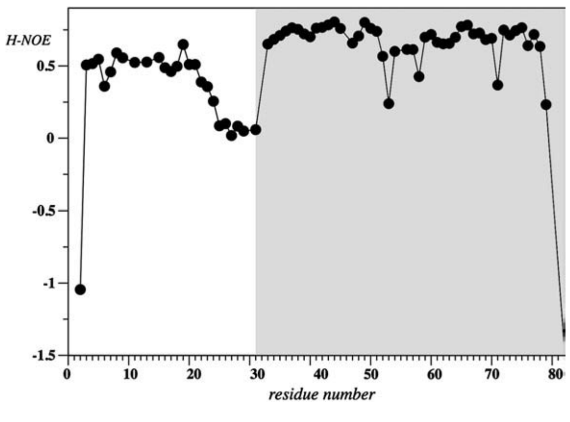

Fig. 7. Values of the $^{15}N\{^{1}H\}$ NOE of full-length Zn_6E_c-1. The segment corresponding to β_E-E_c-1 is shaded in gray.

Discussion

MTs belong to the first proteins that were structurally characterized by NMR in detail.[43] Interestingly, only two crystal structures have been reported so far,[5,41,44] most likely reflecting problems in crystallizing proteins that contain well-folded units separated by flexible hinges and the difficulty of determining the X-ray structure of the protein when structure factors are dominated by the presence of many strongly scattering metal ions.

Among family 1 or vertebrate MTs, solution structures of mouse MT-1;[12] rabbit, rat, and human MT-2;[5,6,8] human[45] and mouse[46] MT-3; and *Notothenia coriiceps* (black rockcod fish) MT[7,12] have been reported. Common to all vertebrate MTs are metal ion coordination sites formed by 20 Cys residues, allowing the binding of a total of seven divalent metal ions arranged in two separated metal–thiolate clusters. A four-metal cluster formed by 11 Cys residues is located in the C-terminal α-domain. The N-terminal β-domain contains a cluster formed by nine cysteines and three metal ions. In case of human or mouse MT-3, the β-domain of the polypeptide chain was too flexible to be structurally characterized.[45,46] The two metal-binding domains are separated by a short conserved linker consisting of Lys-Lys-Ser. Divalent metal ions such as Zn^{II} or Cd^{II} are tetrahedrally coordinated by terminal and bridging thiolate ligands. Two MTs from family 3, which comprises crustacean isoforms, have been described. *Callinectes sapidus* (blue crab) MT-1[10] and *Homarus americanus* (lobster) MT[9] bind six divalent metal ions that are distributed in two M_3Cys_9 metal centers similar to the β-domain of vertebrate MTs. The structure of *Strongylocentrotus purpuratus* (purple sea urchin) MT-A,[11] a member of family 4 (echinodermata), resembles vertebrate isoforms in that seven metal ions are coordinated in M_4Cys_{11} and M_3Cys_9 clusters, but the C- and N-terminal locations of the metal clusters are inverted in the two MT types. The *Saccharomyces cerevisiae* MT has been studied by NMR[47] and also crystallized in its Cu^{I} form.[44] This MT from family 12 (fungi) binds seven to eight Cu^{I} ions in one single domain and contains a total of 12 cysteines, of which only 10 participate in Cu^{I} coordination.[48] In the inorganic core of this protein, two Cu^{I} ions are diagonally coordinated by cysteines, while the others are trigonally coordinated. The fungus *Neurospora crassa* binds six Cu(I) ions in a single-domain architecture via a Cu_6Cys_7 cluster.[49] Finally, the cyanobacterial SmtA protein from family 14 of prokaryotic MTs binds four Zn^{II} ions by nine Cys and two His residues in a single metal cluster[13] with similar topology as the M_4Cys_{11} cluster of the α-domain of the vertebrate MTs. In addition to the finding that His participates in metal coordination, SmtA revealed a high content of well-defined secondary structure that is unusual for MTs. In general, the only regular secondary structural elements present in MTs are short 3_{10}-helices and "half-turns,"[50,51] but SmtA possesses a short α-helix and two small antiparallel β-sheets.

Similar to most MTs described to date, β_E-E_c-1 has little regular secondary structure, except for a single helical turn. Its fold is entirely imposed onto the structure through metal ion coordination. Even the long loop that partially encircles the metal centers of the β_E-domain is devoid of regular secondary structure. The β_E-domain of E_c-1 binds four metal ions in a manner very different from the one in the other MTs that have been structurally characterized so far. The Zn_3Cys_9 metal–thiolate cluster most closely resembles the β-domain found in vertebrate[5,7,12] and invertebrate[9–11] MTs. However, in contrast to the β-domain of these isoforms, the participating Cys residues are relatively far apart from each other in the amino acid sequence. Twenty residues—among them Cys47 and Cys49, which are part of the mononuclear binding site, and residues of the loop encompassing residues Gly50 to Asn64—separate the two Cys-rich stretches that form this trinuclear metal–thiolate cluster. A second important structural aspect of β_E-E_c-1 is the mononuclear binding site formed by His33, His41, Cys47, and Cys49. This makes β_E-E_c-1 the first MT known to contain such a mononuclear binding site.

Histidine imidazole-coordinating metal ions in MTs have already been reported for the cyanobacterial MT SmtA.[52] The latter protein possesses a single $Zn_4Cys_9His_2$ cluster with a topology similar to the one encountered in the M_4Cys_{11} clusters of vertebrate α-domains. Therein, the His residues have been shown to confer specific metal ion-binding properties to the protein.[52] Also other spectroscopic techniques besides NMR give evidence that His residues are involved in metal ion coordination in β_E-E_c-1. Titration of apoE_c-1 with Co^{II} ions, followed by UV–vis spectroscopy, showed that the *d–d* transitions in the visible region contain features that are also found in the spectra of Co^{II}-substituted Zn-finger proteins with one or more histidine ligands.[33] Extended X-ray absorption fine structure spectra of β_E-E_c-1 and full-length E_c-1[34] are consistent with average coordination numbers of 3.5 and 3.8, respectively, for sulphur (Cys), and 0.5 and 0.2, respectively, for lighter ligands, which in this case can be assigned to nitrogen atoms from the imidazole groups, and hence are in full agreement with the solution structure presented here. Further support of this view was provided by mass spectrometry and NMR studies[53] that demonstrated a correlation between the loss of Zn^{II} ions and the protonation state of the histidine residues.

An open question is how this unique metal–thiolate arrangement aids in or even brings about the function of the seed-specific wheat E_c-1, which is primarily thought to fulfill a role in Zn^{II} storage. Mononuclear Cys_2His_2 sites in zinc-finger proteins were shown[26] to bind Zn^{II} stronger (binding constant, 1.8×10^{11} M^{-1}) than Cd^{II} (binding constant, 5.0×10^{8} M^{-1}), underlining a role in Zn^{II} homeostasis rather than heavy metal detoxification. As the mononuclear binding site combines ligands from relatively distant parts of the amino acid sequence, a structure-stabilizing role is feasible. On one hand, this stabilization of loop sequences could affect the stability of the three-metal ion cluster, thereby increasing the Zn^{II} affinity of the protein and suggesting a role as a putative zinc storage protein. On the other hand, the mononuclear site might be important for the formation of a specific structural motif that could be required for a so far unknown function. Such a motif might be required for the recognition of not-yet-identified binding partners of E_c-1 in analogy to zinc-finger proteins, the yeast transcription factor GAL4, a homodimeric protein containing one Zn_2Cys_6 cluster per monomer,[54] or retroviral nucleocapsid proteins, in which so-called zinc-knuckle motifs are primarily involved in RNA interaction.[55,56] Finally, a question arises about the specific functional role of the mononuclear Zn^{II} binding site that, both in its presence and in its ligand composition, is highly unusual for the members of the MT superfamily identified so far. The site may be involved in controlling the release and/or uptake of Zn^{II} ions from the β-type cluster. The relative binding constants to the isolated site and the three-metal cluster all lie in the same range (1.8×10^{11} M^{-1} for $ZnCys_2His_2$ *versus* 2×10^{11} M^{-1} for the Zn_3Cys_9 cluster of the β-domain of human MT2),[57] so that transfer between the two sites may be rapid. Along the same line, it is impossible to selectively remove a single Zn^{II} ion from $Zn_4\beta_E$-E_c-1 with a metal ion chelator. The removal of 1 Eq of Zn^{II} led to destabilization of the entire structure, in accordance with partial metal ion removal from multiple sites within the protein. Alternatively, the isolated metal binding site might be required for docking to a binding partner to enable specific Zn^{II} transfer. Future experiments are needed to further elucidate the function of this protein.

Materials and Methods

Chemicals and solutions

d_{11}-Tris was purchased from Euriso-Top (Saclay, France), and $^{15}NH_4Cl$ and $^{113}CdCl_2$ were purchased from Cambridge Isotope Laboratories (Innerberg, Switzerland). PAR and all other chemicals were bought from Fluka (Buchs, Switzerland). Solutions were prepared with deionized water, which was degassed and nitrogen-saturated when necessary.

NMR sample preparations

The sequence of the C-terminal β_E-E_c-1 domain was derived from proteolytic digestion experiments with the full-length protein using proteinase K.[20] ^{15}N-labeled samples of E_c-1 and β_E-E_c-1 were expressed as C-terminal intein fusions containing an additional maltose-binding domain for affinity purification on chitin beads (New England Biolabs, Ipswich, MA, USA). Expression and purification were performed as described previously in detail, except for the use of M9 minimal growth media for bacterial cultures, which were prepared without addition of Cu^{II} salts.[20] NMR experiments were recorded at 298 K on Bruker Avance 700- and 600-MHz spectrometers using samples containing 1 mM $Zn_4\beta_E$-E_c-1 or 1 mM Zn_6E_c-1 in 15 mM d_{11}-Tris–HCl (pH 6.8) and 50 mM NaCl. Approximately 3 mM $^{113}Cd_4\beta_E$-E_c-1 in the same buffer and salt conditions was prepared by reconstitution of the apo form with $^{113}Cd^{II}$, as described before.

NMR spectroscopy

Assignment of resonances was performed using 3D ^{15}N-resolved NOESY[58,59] and TOCSY[60,61] spectra recorded with mixing times of 200 and 80 ms, respectively. Restraints used in the structure calculation were derived from 120-ms NOESY spectra using both a 3D ^{15}N-resolved experiment and a 2D NOESY experiment. In all cases, zero-quantum interference in the spectra was suppressed using a zero-quantum suppression filter.[62,63] ^{15}N,^{1}H correlation maps were derived from a gradient-enhanced [^{15}N,^{1}H] HSQC experiment using the Rance–Palmer trick for sensitivity enhancement.[64,65] T_1 and T_2 ^{15}N relaxation experiments were recorded using 2D versions of inversion recovery (T_1)[66] and Carr-Purcell-Meiboom-Gill spin-echo[67] experiments. Relaxation rates were derived from least squares fits to peak volumes using the Levenberg–Marquardt algorithm. The ^{15}N{^{1}H} NOE data were derived from steady-state NOE experiments.[68] Proton chemical shifts have been referenced relative to water resonance at 4.73 ppm and 300 K, from which the ^{15}N scale was derived by multiplying the frequency of 0 ppm with 0.10132900.

Assignment

Sequence-specific resonance assignment was performed using the methodology developed by Wüthrich.[69] Assignments were achieved based on information from 2D TOCSY, NOESY, 2D [^{15}N,^{1}H]HSQC, 3D [^{15}N]NOESY, and 3D [^{15}N]TOCSY experiments. The 2D and 3D spectra were evaluated with the programs XEASY[70] and CARA,[71] respectively. As a first step, the spin systems were identified in the 2D TOCSY or 3D [^{15}N]TOCSY experiments. Subsequently, spin systems were linked based on NOE information derived from 2D NOESY and 3D [^{15}N] NOESY. A "sequential walk" is shown in Fig. S1 of Supplementary Material. Once longer stretches had been identified, they were mapped onto the sequence of β_E-E_c-1. The ^{15}N{^{1}H} NOE data were useful in recognizing residues from the terminal positions early on.

Metal ion coordination determination

On the basis of automated NOE assignment and structure calculations without metal ions (Supplementary Material, Fig. S3), it was clear that a single metal ion is coordinated by His33 $N^{\delta1}$, His41 $N^{\varepsilon2}$, Cys47 S^{γ}, and Cys49 S^{γ}. The different coordination modes of His33 and His41 were additionally confirmed by [^{15}N,^{1}H]HSQC spectra optimized for long-range couplings (Fig. S4).[72,73] The remaining nine Cys residues can form a cluster with three equivalent metal ions, three bridging Cys (binding two metal ions each), and 3×2 terminal Cys (binding one metal ion each) in $(9\times8\times7)/6\times(6\times5)/2\times(4\times3)/2\times(2\times1)/2=7560$ different ways, excluding symmetrically related arrangements. For any given cluster coordination, the geometry of the three-metal cluster was fixed by upper and lower distance bounds of $3.75\leq d(\text{Zn, Zn})\leq4.0$ Å between the metal ions (three restraints), $d(\text{Zn, S}^{\gamma})=2.3$ Å and $3.3\leq d(\text{Zn, C}_{\beta})\leq3.5$ Å between a metal ion and its four coordinating Cys (24 restraints), and $d(\text{S}^{\gamma}, \text{S}^{\gamma})=3.77$ Å between Cys residues that coordinate the same metal ion (18 restraints). Similar distances were used to restrain the mononuclear $ZnCys_2$-His_2 cluster. Using the program CYANA, we performed, for each of the 7560 possible cluster arrangements, a complete structure calculation with automated NOE assignment and three structure calculations with the NOE upper distance limits resulting from three automated NOE assignment and structure calculations without metal ions that were started from different randomized initial structures. Structure calculations were performed on a Linux cluster system. Up to 100 processors were used in parallel to complete the computations in about 4 days.

Table 1. Structural statistics for the β_E-domain of E_c-1 MT

NMR distance restraints	
Total NOE	539
Short range: $\lvert i-j\rvert\leq1$	321
Medium range: $1<\lvert i-j\rvert<5$	106
Long range: $\lvert i-j\rvert\geq5$	112
Maximal distance restraint violation (Å)	0.13
AMBER energies (kcal/mol)	
Total (mean±SD of 20 conformers)	−1518±118kcal/mol
van der Waals	−44±10kcal/mol
RMSDs from idealized geometry	
Bond lengths (Å)	0.0150±0.0002
Bond angles (°)	2.39±0.06
Ramachandran plot statistics[81] (%)	
Residues in most favored regions	63.8
Residues in additionally allowed regions	32.1
Residues in generously allowed regions	3.1
Residues in disallowed regions	1.0
RMSDs from the mean coordinates (Å)	
N, C^{α}, and C′ of residues 32–77	0.60±0.14
Heavy atoms of residues 32–77	1.13±0.14

Structure calculation

The automated NOE assignment[74] and the structure calculation with torsion angle dynamics[75] were performed with the program CYANA 3.0.[76] Structure calculations were started from 100 conformers with randomized torsion angle values. Eight thousand torsion angle dynamics steps were performed per conformer, and the 20 conformers with the lowest final target function value were retained for analysis. Automated NOE assignment comprised seven cycles of combined automated NOE assignment and structure calculation, and a final structure calculation using only NOE distance restraints with unambiguous assignment. The final 20 CYANA conformers with the lowest target function values were subjected to restrained energy minimization in explicit solvent against the AMBER force field[77] using the program OPALp.[78,79] Structure figures were generated with the program MOLMOL.[80] Structural statistics are shown in Table 1.

Zn^{II} competition experiments

A sample of 220 μM $Zn_4\beta_E$-E_c-1 in 15 mM d_{11}-Tris–HCl (pH 6.8) and 50 mM NaCl was mixed with 27.1 mM PAR, and the metal ion competition reaction was followed with [^{15}N,^{1}H]HSQC experiments. In addition, the same reaction was followed with UV spectroscopy using an analogously prepared sample. The amount of Zn^{II} ions released from the β_E-domain was calculated from absorption at 500 nm using a molar absorptivity value of the $Zn(PAR)_2$ complex at pH 6.8 of ε_{500}=21,170 M^{-1} cm^{-1}, which was determined experimentally.

Accession codes

The coordinates of the 20 energy-refined CYANA conformers of $Zn_4\beta_E$-E_c-1 and the conformational restraints for the structure calculation have been deposited in the Protein Data Bank with accession code 2KAK. The chemical shifts have been deposited in the Biological Magnetic Resonance Bank with accession number 16025.

Acknowledgements

We thank Alexey Neumoin for technical support during spectra assignment. This work was supported by the Swiss National Science Foundation (SNF grant 200020-113728/1 and SNF Förderungsprofessur PP002-119106/1 to E.F.), the Volkswagen Foundation (Lichtenberg Professorship to P.G.), and a Grant-in-Aid for Scientific Research of the Japan Society for the Promotion of Science (P.G.). The authors deeply acknowledge continuous discussions with Milan Vašák.

Supplementary Data

Supplementary data associated with this article can be found, in the online version, at doi:10.1016/j.jmb.2009.01.035

References

1. Binz, P. A. & Kägi, J. H. R. (1999). In *Metallothionein IV* (Klaassen, C., ed.), pp. 7–13, Birkhäuser Verlag, Basel.
2. Coyle, P., Philcox, J. C., Carey, L. C. & Rofe, A. M. (2002). Metallothionein: the multipurpose protein. *Cell. Mol. Life Sci.* **59**, 627–647.
3. Palmiter, R. D. (1998). The elusive function of metallothionein. *Proc. Natl Acad. Sci. USA*, **95**, 8428–8430.
4. Bernhard, W. R., Vašák, M. & Kägi, J. H. R. (1986). Cadmium binding and metal cluster formation in metallothionein: a differential modification study. *Biochemistry*, **25**, 1975–1980.
5. Braun, W., Vašák, M., Robbins, A. H., Stout, C. D., Wagner, G., Kägi, J. H. R. & Wüthrich, K. (1992). Comparison of the NMR solution structure and the X-ray crystal structure of rat metallothionein-2. *Proc. Natl Acad. Sci. USA*, **89**, 10124–10128.
6. Arseniev, A., Schultze, P., Wörgötter, E., Braun, W., Wagner, G., Vašák, M. *et al.* (1988). Three-dimensional structure of rabbit liver [Cd_7]metallothionein-2a in aqueous solution determined by nuclear magnetic resonance. *J. Mol. Biol.* **201**, 637–657.
7. Capasso, C., Carginale, V., Crescenzi, O., Di Maro, D., Parisi, E., Spadaccini, R. & Temussi, P. A. (2003). Solution structure of MT_nc, a novel metallothionein from the Antarctic fish *Notothenia coriiceps*. *Structure*, **11**, 435–443.
8. Messerle, B. A., Schaffer, A., Vašák, M., Kägi, J. H. R. & Wüthrich, K. (1990). Three-dimensional structure of human $^{113}Cd_7$metallothionein-2 in solution determined by nuclear magnetic resonance spectroscopy. *J. Mol. Biol.* **214**, 765–779.
9. Munoz, A., Forsterling, F. H., Shaw, C. F., III & Petering, D. H. (2002). Structure of the $^{113}Cd_3$beta domains from *Homarus americanus* metallothionein-1: hydrogen bonding and solvent accessibility of sulfur atoms. *J. Biol. Inorg. Chem.* **7**, 713–724.
10. Narula, S. S., Brouwer, M., Hua, Y. & Armitage, I. M. (1995). Three-dimensional solution structure of *Callinectes sapidus* metallothionein-1 determined by homonuclear and heteronuclear magnetic resonance spectroscopy. *Biochemistry*, **34**, 620–631.
11. Riek, R., Precheur, B., Wang, Y., Mackay, E. A., Wider, G., Güntert, P. *et al.* (1999). NMR structure of the sea urchin (*Strongylocentrotus purpuratus*) metallothionein MTA. *J. Mol. Biol.* **291**, 417–428.
12. Zangger, K., Öz, G., Otvos, J. D. & Armitage, I. M. (1999). Three-dimensional solution structure of mouse [Cd_7]-metallothionein-1 by homonuclear and heteronuclear NMR spectroscopy. *Protein Sci.* **8**, 2630–2638.
13. Blindauer, C. A., Harrison, M. D., Parkinson, J. A., Robinson, A. K., Cavet, J. S., Robinson, N. J. & Sadler, P. J. (2001). A metallothionein containing a zinc finger within a four-metal cluster protects a bacterium from zinc toxicity. *Proc. Natl Acad. Sci. USA*, **98**, 9593–9598.
14. Abdullah, S. N. A., Cheah, S. C. & Murphy, D. J. (2002). Isolation and characterisation of two divergent type 3 metallothioneins from oil palm, *Elaeis guineensis*. *Plant Physiol. Biochem.* **40**, 255–263.
15. Reynolds, T. L. & Crawford, R. L. (1996). Changes in abundance of an abscisic acid-responsive, early cysteine-labeled metallothionein transcript during pollen embryogenesis in bread wheat (*Triticum aestivum*). *Plant Mol. Biol.* **32**, 823–829.
16. Hanley-Bowdoin, L. & Lane, B. G. (1983). A novel protein programmed by the mRNA conserved in dry wheat embryos. The principal site of cysteine incor-

poration during early germination. *Eur. J. Biochem.* **135**, 9–15.
17. Kawashima, I., Kennedy, T. D., Chino, M. & Lane, B. G. (1992). Wheat E_c metallothionein genes—like mammalian Zn^{2+} metallothionein genes, wheat Zn^{2+} metallothionein genes are conspicuously expressed during embryogenesis. *Eur. J. Biochem.* **209**, 971–976.
18. Lane, B. G., Kajioka, R. & Kennedy, T. D. (1987). The wheat-germ E_c protein is a zinc-containing metallothionein. *Biochem. Cell Biol.* **65**, 1001–1005.
19. Ozturk, L., Yazici, M. A., Yucel, C., Torun, A., Cekic, C., Bagci, A. *et al.* (2006). Concentration and localization of zinc during seed development and germination in wheat. *Physiol. Plant.* **128**, 144–152.
20. Peroza, E. A. & Freisinger, E. (2007). Metal ion binding properties of *Triticum aestivum* E_c-1 metallothionein: evidence supporting two separate metal–thiolate clusters. *J. Biol. Inorg. Chem.* **12**, 377–391.
21. Schultze, P., Wörgötter, E., Braun, W., Wagner, G., Vašák, M., Kägi, J. H. R. & Wührich, K. (1988). Conformation of [Cd_7]-metallothionein-2 from rat liver in aqueous solution determined by nuclear magnetic resonance spectroscopy. *J. Mol. Biol.* **203**, 251–268.
22. Frey, M. H., Wagner, G., Vašák, M., Soerensen, O. W., Neuhaus, D., Wörgötter, E. *et al.* (1985). Polypeptide metal cluster connectivities in metallothionein-2 by novel H-1-Cd-113 heteronuclear two-dimensional NMR experiments. *J. Am. Chem. Soc.* **107**, 6847–6851.
23. Live, D., Armitage, J. M., Dalgarno, D. C. & Cowburn, D. (1985). Two-dimensional ^{1}H–^{113}Cd chemical shift correlation maps by ^{1}H-detected multiple-quantum NMR in metal complexes and metalloproteins. *J. Am. Chem. Soc.* **107**, 1775–1777.
24. Otvos, J. D., Engeseth, H. R. & Wehrli, S. (1985). Multiple-quantum ^{113}Cd–^{1}H correlation spectroscopy as a probe of metal coordination environments in metalloproteins. *J. Magn. Reson.* **61**, 579–584.
25. Herrmann, T., Güntert, P. & Wüthrich, K. (2002). Protein NMR structure determination with automated NOE assignment using the new software CANDID and the torsion angle dynamics algorithm DYANA. *J. Mol. Biol.* **319**, 209–227.
26. Krizek, B. A., Merkle, D. L. & Berg, J. M. (1993). Ligand variation and metal ion binding specificity in zinc finger peptides. *Inorg. Chem.* **32**, 937–940.
27. Kägi, J. H. R. (1991). Overview of metallothionein. *Methods Enzymol.* **205**, 613–626.
28. Nettesheim, D. G., Engeseth, H. R. & Otvos, J. D. (1985). Products of metal exchange reactions of metallothionein. *Biochemistry*, **24**, 6744–6751.
29. Vašák, M. & Bogumil, R. (1997). In *Cytotoxic, Mutagenic and Carcinogenic Potential of Heavy Metals Related to Human Environment* (Hadjiliadis, N. D., ed.), pp. 195–215, Kluwer, Dordrecht, The Netherlands.
30. Briggs, R. W. & Armitage, I. M. (1982). Evidence for site-selective metal binding in calf liver metallothionein. *J. Biol. Chem.* **257**, 1259–1262.
31. Otvos, J. D., Liu, X., Li, H., Shen, G. & Basti, M. (1993). In *Metallothionein III* (Suzuki, K. T., Imura, N. & Kimura, M., eds), pp. 57–74, Birkhäuser, Basel.
32. Maret, W., Larsen, K. S. & Vallee, B. L. (1997). Coordination dynamics of biological zinc "clusters" in metallothioneins and in the DNA-binding domain of the transcription factor Gal4. *Proc. Natl Acad. Sci. USA*, **94**, 2233–2237.
33. Faller, P., Hasler, D. W., Zerbe, O., Klauser, S., Winge, D. R. & Vašák, M. (1999). Evidence for a dynamic structure of human neuronal growth inhibitory factor and for major rearrangements of its metal–thiolate clusters. *Biochemistry*, **38**, 10158–10167.
34. Peroza, E. A., Al Kaabi, A., Meyer-Klaucke, W., Wellenreuther, G., Freisinger, E. The two distinctive metal ion binding domains of the wheat metallothionein E_c-1. *J. Inorg. Biochem.* doi:10.1016/j.jinorgbio.2008.11.008, in press.
35. Schicht, O. & Freisinger, E., Spectroscopic characterization of *Cicer arietinum* metallothionein 1. *Inorg. Chim. Acta*, **362**, 714–724.
36. Shaw, C. F., III, Stillman, M. J. & Suzuki, K. T. (1992). Metallothioneins: Synthesis, Structure and Properties of Metallothioneins, Phytochelatins and Metal–Thiolate Complexes, VCH Publishers, New York.
37. Byrd, J. & Winge, D. R. (1986). Cooperative cluster formation in metallothionein. *Arch. Biochem. Biophys.* **250**, 233–237.
38. Nielson, K. B. & Winge, D. R. (1983). Order of metal binding in metallothionein. *J. Biol. Chem.* **258**, 13063–13069.
39. Good, M., Hollenstein, R., Sadler, P. J. & Vašák, M. (1988). Cd-113 NMR-studies on metal thiolate cluster formation in rabbit Cd(II)-metallothionein—evidence for a pH-dependence. *Biochemistry*, **27**, 7163–7166.
40. Sutherland, D. E. K. & Stillman, M. J. (2008). Noncooperative cadmium(II) binding to human metallothionein la. *Biochem. Biophys. Res. Commun.* **372**, 840–844.
41. Robbins, A. H., McRee, D. E., Williamson, M., Collett, S. A., Xuong, N. H., Furey, W. F. *et al.* (1991). Refined crystal structure of Cd, Zn metallothionein at 2.0 Å resolution. *J. Mol. Biol.* **221**, 1269–1293.
42. Zangger, K. & Armitage, I. M. (2002). Dynamics of interdomain and intermolecular interactions in mammalian metallothioneins. *J. Inorg. Biochem.* **88**, 135–143.
43. Wüthrich, K. (1991). Determination of the three-dimensional structure of metallothioneins by nuclear magnetic resonance spectroscopy in solution. *Methods Enzymol.* **205**, 502–520.
44. Calderone, V., Dolderer, B., Hartmann, H. J., Echner, H., Luchinat, C., Del Bianco, C. *et al.* (2005). The crystal structure of yeast copper thionein: the solution of a long-lasting enigma. *Proc. Natl Acad. Sci. USA*, **102**, 51–56.
45. Wang, H., Zhang, Q., Cai, B., Li, H., Sze, K. H., Huang, Z. X. *et al.* (2006). Solution structure and dynamics of human metallothionein-3 (MT-3). *FEBS Lett.* **580**, 795–800.
46. Öz, G., Zangger, K. & Armitage, I. M. (2001). Three-dimensional structure and dynamics of a brain specific growth inhibitory factor: metallothionein-3. *Biochemistry*, **40**, 11433–11441.
47. Peterson, C. W., Narula, S. S. & Armitage, I. M. (1996). 3D solution structure of copper and silver-substituted yeast metallothioneins. *FEBS Lett.* **379**, 85–93.
48. Luchinat, C., Dolderer, B., Del Bianco, C., Echner, H., Hartmann, H. J., Voelter, W. & Weser, U. (2003). The Cu^{I}_{7} cluster in yeast copper thionein survives major shortening of the polypeptide backbone as deduced from electronic absorption, circular dichroism, luminescence and H-1 NMR. *J. Biol. Inorg. Chem. I*, **8**, 353–359.
49. Cobine, P. A., McKay, R. T., Zangger, K., Dameron, C. T. & Armitage, I. M. (2004). Solution structure of Cu_6 metallothionein from the fungus *Neurospora crassa*. *Eur. J. Biochem.* **271**, 4213–4221.

50. Braun, W., Wagner, B., Wörgötter, E., Vašák, M., Kägi, J. H. R. & Wüthrich, K. (1986). Nuclear magnetic resonance identification of "half-turn" and 3_{10}-helix secondary structure in rabbit liver metallothionein-2. *J. Mol. Biol.* **187**, 131–135.
51. Braun, W., Wagner, B., Wörgötter, E., Vašák, M., Kägi, J. H. R. & Wüthrich, K. (1986). Polypeptide fold in the two metal clusters of metallothionein-2 by nuclear magnetic resonance in solution. *J. Mol. Biol.* **197**, 125–129.
52. Blindauer, C. A., Razi, M. T., Campopiano, D. J. & Sadler, P. J. (2007). Histidine ligands in bacterial metallothionein enhance cluster stability. *J. Biol. Inorg. Chem.* **12**, 393–405.
53. Leszczyszyn, O. I., Schmid, R. & Blindauer, C. A. (2007). Toward a property/function relationship for metallothioneins: histidine coordination and unusual cluster composition in a zinc-metallothionein from plants. *Proteins*, **68**, 922–935.
54. Pan, T. & Coleman, J. E. (1990). GAL4 transcription factor is not a "zinc finger" but forms a $Zn(II)_2Cys_6$ binuclear cluster. *Proc. Natl Acad. Sci. USA*, **87**, 2077–2081.
55. Klein, D. J., Johnson, P. E., Zollars, E. S., De Guzman, R. N. & Summers, M. F. (2000). The NMR structure of the nucleocapsid protein from the mouse mammary tumor virus reveals unusual folding of the C-terminal zinc knuckle. *Biochemistry*, **39**, 1604–1612.
56. De Guzman, R. N., Wu, Z. R., Stalling, C. C., Pappalardo, L., Borer, P. N. & Summers, M. F. (1998). Structure of the HIV-1 nucleocapsid protein bound to the SL3 psi-RNA recognition element. *Science*, **279**, 384–388.
57. Jiang, L. J., Vašák, M., Vallee, B. L. & Maret, W. (2000). Zinc transfer potentials of the alpha- and beta-clusters of metallothionein are affected by domain interactions in the whole molecule. *Proc. Natl Acad. Sci. USA*, **97**, 2503–2508.
58. Kumar, A., Ernst, R. R. & Wüthrich, K. (1980). A two-dimensional nuclear Overhauser enhancement (2D NOE) experiment for the elucidation of complete proton–proton cross-relaxation networks in biological macromolecules. *Biochem. Biophys. Res. Commun.* **95**, 1–6.
59. Macura, S. & Ernst, R. R. (1980). Elucidation of cross-relaxation in liquids by two-dimensional NMR spectroscopy. *Mol. Phys.* **41**, 95–117.
60. Braunschweiler, L. & Ernst, R. R. (1983). Coherence transfer by isotropic mixing: application to proton correlation spectroscopy. *J. Magn. Reson.* **53**, 521–528.
61. Bax, A. & Davis, D. G. (1985). MLEV17-based two-dimensional homonuclear magnetization transfer spectroscopy. *J. Magn. Reson.* **65**, 355–360.
62. Otting, G. (1990). Zero-quantum suppression in NOESY and experiments with a z-filter. *J. Magn. Reson.* **86**, 496–508.
63. Rance, M., Bodenhausen, G., Wagner, G., Wüthrich, K. & Ernst, R. R. (1985). A systematic approach to the suppression of *J* cross peaks in 2D exchange and 2D NOE spectroscopy. *J. Magn. Reson.* **62**, 497–510.
64. Palmer, A. G., Cavanagh, J., Wright, P. E. & Rance, M. (1991). Sensitivity improvement in proton-detected two-dimensional heteronuclear correlation NMR spectroscopy. *J. Magn. Reson.* **93**, 151–170.
65. Kay, L. E., Keifer, P. & Saarien, T. (1992). Pure absorption gradient enhanced heteronuclear single-quantum correlation spectroscopy with improved sensitivity. *J. Am. Chem. Soc.* **114**, 10663–10665.
66. Vold, R. L. & Vacca, J. P., Measurement of spin-relaxation rates in complex systems. J. Chem. Phys. 48, 3831–3832.
67. Meiboom, S. & Gill, D. (1958). Modified spin-echo method for measuring spin-relaxation rates. *Rev. Sci. Instrum.* **29**, 688–691.
68. Noggle, J. H. & Schirmer, R. E. (1971). The Nuclear Overhauser Effect—Chemical Applications Academic Press, New York.
69. Wüthrich, K. (1986). NMR of Proteins and Nucleic Acids Wiley-Interscience, New York.
70. Bartels, C., Xia, T. H., Billeter, M., Güntert, P. & Wüthrich, K. (1995). The program XEASY for computer-supported spectral analysis of biological macromolecules. *J. Biomol. NMR*, **6**, 1–10.
71. Keller, R. (2004). The Computer Aided Resonance Assignment Tutorial CANTINA Verlag, Goldau.
72. Drohat, A. C., Xiao, G., Tordova, M., Jagadeesh, J., Pankiewicz, K. W., Watanabe, K. A. *et al.* (1999). Heteronuclear NMR and crystallographic studies of wild-type and H187Q *Escherichia coli* uracil DNA glycosylase: electrophilic catalysis of uracil expulsion by a neutral histidine 187. *Biochemistry*, **38**, 11876–11886.
73. Pelton, J. G., Torchia, D. A., Meadow, N. D. & Roseman, S. (1993). Tautomeric states of the active-site histidines of phosphorylated and unphosphorylated IIIGlc, a signal-transducing protein from *Escherichia coli*, using two-dimensional heteronuclear NMR techniques. *Protein Sci.* **2**, 543–558.
74. Herrmann, T., Güntert, P. & Wüthrich, K. (2002). Protein NMR structure determination with automated NOE-identification in the NOESY spectra using the new software ATNOS. *J. Biomol. NMR*, **24**, 171–189.
75. Güntert, P., Mumenthaler, C. & Wüthrich, K. (1997). Torsion angle dynamics for NMR structure calculation with the new program DYANA. *J. Mol. Biol.* **273**, 283–298.
76. Güntert, P. (2003). Automated NMR protein structure calculation. *Progr. Nucl. Magn. Reson. Spectrosc.* **43**, 105–125.
77. Cornell, W. D., Cieplak, P., Bayly, C. I., Gould, I. R., Merz, K. M., Ferguson, D. M. *et al.* (1995). A second generation force field for the simulation of proteins, nucleic acids, and organic molecules. *J. Am. Chem. Soc.* **118**, 5179–5197.
78. Koradi, R., Billeter, M. & Güntert, P. (2000). Point-centered domain decomposition for parallel molecular dynamics simulation. *Comput. Phys. Commun.* **124**, 139–147.
79. Luginbühl, P., Güntert, P., Billeter, M. & Wüthrich, K. (1996). The new program OPAL for molecular dynamics simulations and energy refinements of biological macromolecules. *J. Biomol. NMR*, **8**, 136–146.
80. Koradi, R., Billeter, M. & Wüthrich, K. (1996). MOLMOL: a program for display and analysis of macromolecular structures. *J. Mol. Graphics*, **14**, 51–55.
81. Laskowski, R. A., Rullmann, J. A. C., Macarthur, M. W., Kaptein, R. & Thornton, J. M. (1996). Aqua and Procheck-NMR—programs for checking the quality of protein structures solved by NMR. *J. Biomol. NMR*, **8**, 477–486.